Numerical Analysis of Hydrodynamics Around Submarine Pipeline End Manifold (PLEM) Under Tsunami-Like Wave

Article *in* IEEE Access · December 2019

DOI: 10.1109/ACCESS.2019.2957395

4 authors, including:

Enjin Zhao
China University of Geosciences
65 PUBLICATIONS **606** CITATIONS
SEE PROFILE

Lin Mu
Shenzhen University
133 PUBLICATIONS **1,826** CITATIONS
SEE PROFILE

IEEE Access
Multidisciplinary | Rapid Review | Open Access Journal

Received October 24, 2019, accepted November 19, 2019, date of publication December 3, 2019,
date of current version December 23, 2019.

Digital Object Identifier 10.1109/ACCESS.2019.2957395

Numerical Analysis of Hydrodynamics Around Submarine Pipeline End Manifold (PLEM) Under Tsunami-Like Wave

ENJIN ZHAO[1,3,4], YUEZHAO TANG[1], JIE SHAO[5], AND LIN MU[2,3]

[1]College of Marine Science and Technology, China University of Geosciences, Wuhan 430074, China
[2]College of Life Sciences and Oceanography, Shenzhen University, Shenzhen 518060, China
[3]Southern Marine Science and Engineering Guangdong Laboratory (Guangzhou), Guangzhou 511458, China
[4]Shenzhen Research Institute, China University of Geosciences, Shenzhen 518057, China
[5]Zhejiang Institute of Hydraulics and Estuary, Hangzhou 310020, China

Corresponding author: Lin Mu (moulin1977@hotmail.com)

This work was supported in part by the National Key Research and Development Program of China under Grant 2017YFC1404700, in part by the Talent Team Introduction Project of Southern Marine Science and Engineering Guangdong Laboratory (Guangzhou) under Grant GML2019ZD0604, in part by the Natural Science Fund of Zhejiang Province under Grant LQ16E090004, in part by the Discipline Layout Project for Basic Research of Shenzhen Science and Technology Innovation Committee under Grant 20170418, and in part by the Guangdong Special Fund Program for Economic Development (Marine Economic) under Grant GDME-2018E001.

ABSTRACT Submarine Pipeline End Manifold (PLEM) is the converge end or termination of submarine pipelines, which is used to provide additional support for equipment in the submarine production system on the seafloor. However, PLEM is vulnerable to extreme waves (i.e., tsunami waves). In this study, a two-phase flow model is developed with the finite volume method for simulating the tsunami-like wave impinging on the PLEM. Depending on the real-world tsunami wave recorded in 2011 tsunami event, a tsunami-like wave is generated numerically depending on N-waves theory. In order to ensure the accuracy of the calculation, this model is verified against some theoretical and experimental studies firstly. Then, the hydrodynamic characteristics and forces on the PLEMs under the different tsunami-like waves are investigated systematically. Due to the flow causes strong disturbance to different parts of the PLEMs, the Fast Fourier Transform (FFT) method is adopted to analyze the irregular hydrodynamic force signals for better to understand the characteristics of forces in the frequency domain. In the simulations, different environmental and PLEM structural variables are considered, such as wave height, pipe distance, and PLEM bottom seat length. The hydrodynamic characteristics under different tsunami-like waves passing the various submarine PLEMs are discussed, which indicates that the vortex field evolutions and hydrodynamic forces under different waves on the PLEM are significantly different.

INDEX TERMS Tsunami-like wave, submarine pipeline end manifold (PLEM), hydrodynamic forces, flow field, vortex.

I. INTRODUCTION

Due to submarine earthquakes, landslides, volcanic and other disturbances above or below the seawater, a substantial volume of water might fluctuate severely which would induce a series of water waves. The wave height increases while the wavelength and speed decrease when the water wave spreads to shallow sea and coastal area, resulting in the phenomenon of tsunami. Since the tsunami waves are fast, high and strong, it can cause severe damages to industrial equipment, buildings, and offshore structures, leading to huge losses [1], [2]. For example, the tsunami event that happened in Japan in 2011 brought about destructions of 30% of the responding industrial facilities and 7% of the surveyed hazardous materials facilities [3]. On 22 December 2018, a tsunami that followed an eruption and partial collapse of the Anak Krakatau volcano in the Sunda Strait struck several coastal regions of Banten in Java and Lampung in Sumatra, Indonesia. At least 426 people were killed and 14,059 were injured. Therefore, it is urgent to understand the fundamental damaging mechanisms to increase the resilience of the infrastructures during tsunami events [4], [5]. Owing to the

The associate editor coordinating the review of this manuscript and approving it for publication was Haiyong Zheng.

unpredictable nature of a tsunami event, it is difficult to conduct a field experiment. Thus, most of the studies on that topic were carried out by the physical experiments and numerical simulations.

In some studies, solitary wave is employed as the tsunami wave due to the two waves have some similarities in form and stability Aniel-Quiroga *et al.* [6] conducted a series of laboratory experiments on scaled models of two typical Mediterranean rubble-mound breakwater typologies under tsunami waves. In this research, the action of tsunami wave was split into two parts: (1) the first impact of tsunami wave was caused by a large solitary wave; (2) the subsequent overflow was approached by applying a pump-driven wavemaker. Ha *et al.* [7] studied three-dimensional numerical simulation of solitary wave using the immersed boundary (IB) method. Maza *et al.* [8] investigated the interaction between the mangrove forests and the solitary wave instead of the tsunami wave. However, the survey of the real-world tsunami wave indicates that solitary waves rarely happen in the tsunami events. Besides, the evolution of the tsunami wave is completely different from solitary wave at the temporal and spatial scales [9]. Hence, there are some limitations in studying the impact of solitary wave instead of tsunami wave on structures. As a good description of the profile for the tsunami wave could be sufficient to provide a reasonable estimation of the impact on the marine structures, such as submarine pipeline, submarine mudmat, and offshore platform. The tsunami wave which is recorded at the Iwate South station in the 2011 Tohoku Japan tsunami event is observed as a leading-depression wave firstly which induces the decrease of sea level. Then, with the propagation of the tsunami wave, the elevation of the wave surface increases depending on the profile of the tsunami waves. In order to describe the 2011 Japan tsunami wave reasonably, according to the N-waves theory, the tsunami wave recorded at Iwate South station is calculated and replicated using a combination of three $\mathrm{sech}^2(*)$ profiles.

In order to reveal the effects of the tsunami wave on the marine structures, the proposed real-world tsunami-like wave is employed to investigate the tsunami waves impacting on Submarine Pipeline End Manifold (PLEM). Under the tsunami waves, the hydrodynamic loads of PLEM might exceed the design limit instantaneously, leading to irreversible strength damage or loss of overall balance of structures [10] Therefore, to study on hydrodynamic characteristics of PLEMs under tsunami waves is gradually attracted to by researchers. Wang *et al.* [11] proposed a mathematical model for the optimal layout of cluster manifolds with PLEMs under extreme marine conditions. Nam *et al.* [12] carried out experimental and numerical study on coupled motion responses of a floating crane vessel and a lifted subsea manifold in deep water. Wang *et al.* [13] developed a mathematical model of installation process of subsea manifold to analyze the displacement of subsea manifold under different factors.

However, existing researches seldom consider the hydrodynamic characteristics of interaction between tsunami waves and PLEMs using real-world tsunami waves. Besides, since the tsunami wave and solitary wave are quite unlike, the effect of real-world tsunami wave on the offshore structures also differs from that of solitary wave. This paper focuses on this point using CFD simulation method, in which the effects of the real-world tsunami-like wave acting on PLEMs are analyzed and discussed in detail. The numerical model in this paper solves the incompressible Navier-Stokes equations discretized with Finite Volume Method (FVM), and the free surface is captured using the Volume of Fluid (VOF) method. The numerical model is verified in two cases. The systematic study of the real-world tsunami-like wave acting on PLEMs is conducted after the validations. The comparison of the hydrodynamic characteristics under different tsunami-like waves is given, demonstrating remarkable differences in the wave impinging forces. Furthermore, the effects of tsunami-like wave on different PLEMs are also investigated, from which meaningful conclusions are summed up.

II. MODEL DESCRIPTION

A. NUMERICAL SOLVER OF FLUID DOMAIN

The Reynolds Averaged Naiver-Stokes (RANS) solver is adopted to simulate the unsteady incompressible viscous flows with a free surface. The governing equations in the vector form can be written as

$$\nabla \cdot \mathbf{u} = 0 \tag{1}$$

$$\frac{\rho \partial \mathbf{u}}{\partial t} + \rho \nabla \cdot (\mathbf{u}\mathbf{u}) = \nabla \cdot (\mu \nabla \mathbf{u}) + \nabla \mathbf{u} \cdot \nabla \mu - \nabla p + \rho_r \cdot \mathbf{g} \tag{2}$$

where ∇ is the gradient operator, $\mathbf{u}$ is the water velocity vector, ρ is the density, t is the time, μ is effective viscosity including laminar and turbulence viscosity (μ_l and μ_t), p is the pressure, ρ_r is the reference density, $\mathbf{g}$ is the gravity acceleration.

Considering the effect of the turbulence on the PLEMs, the classic Smagorinsky turbulence model is adopted, which has been successfully applied in predicting the wave forces on marine structures and wave breaking process [7], [14]. With this model, the turbulent viscosity is calculated as

$$\mu_t = C^2 (V^{1/3})^2 \sqrt{(\partial u_i/\partial f_j + \partial u_j/\partial f_i)^2/2} \tag{3}$$

where $C = 0.18$ is a constant coefficient which is determined by model validation, V is the control cell volume, u and f are velocity and coordinate, respectively, at the i (x, y, z) or $j(x, y, z)$ spatial coordinate location.

The interface between water and air can be defined by transportation equations of volume of fluid (VOF) as

$$\partial \gamma/\partial t + \nabla \cdot (\gamma \mathbf{u}) = 0 \tag{4}$$

where γ is the volume fraction which is defined by whether the grid control volume is filled by water or air

$\gamma = 0$, $0 < \gamma < 1$ and $\gamma = 1$ represent the air, interface and water in the grid cell, respectively.

The local density and laminar viscosity is calculated depending on the volume fraction.

$$s = s_{air} + \gamma \cdot (s_{water} - s_{air}) \tag{5}$$

where s presents local density ρ or laminar viscosity μ_l.

The non-staggered finite volume method is used over all mesh system [15]. In the simulation, the convective term is discretized depending on the TVD type scheme combing the first-order upwind scheme and the second-order Gamma scheme. Both the diffusion term and pressure gradient term are approximated as the central difference by using values at the auxiliary nodes. The velocities at the faces of the control cell are interpolated from those at the center of the control cell using the momentum interpolation for coupling the governing equations (RANS). And then, the velocity and pressure are resolved using the Pressure Implicit Split Operator (PISO) method. An adaptive time step size was determined from gravity, convective and viscous terms and the Switching Technique for Advection and Capturing of Surfaces (STACS) was used to keep the sharpness of the free surface.

B. WAVE GENERATION METHOD

Solitary waves and tsunami-like waves are numerically generated depending on the dynamic mesh technology. The wave elevation η of solitary waves on a still water depth h could be formulated as

$$\eta(x, t) = H\mathrm{sech}^2[k(x - x_o - Ct)] \tag{6}$$

where H is the wave height; k is the effective number; x_o is the wave peak location at initial time t; C is the wave speed.

Depending on N-waves theory, the tsunami-like wave is numerically generated using a combination of three solitary $\mathrm{sech}^2(*)$ wave profiles [16]–[21]. And the combination wave can be expressed as

$$\begin{aligned}\eta(x_i, t) &= \sum_{i=1}^{3} H_i\mathrm{sech}^2[k_i C_i(t - t_o - t_i)] \\ &= \sum_{i=1}^{3} H_i\mathrm{sech}^2[\omega_i(t - t_o - t_i)]\end{aligned} \tag{7}$$

where H_i, k_i, C_i, t_i and ω_i are the wave elevation, effective number, reference time and wave frequency corresponding to the parameters of the three different combination solitary waves, respectively. The parameters are normalized as follows.

$$\begin{aligned}(H_1/H_o, \omega_1/\omega_o, t_1/T_o) &= (-0.119, 0.0856, 6.556) \\ (H_2/H_o, \omega_2/\omega_o, t_2/T_o) &= (0.328, 0.0947, 8.776) \\ (H_3/H_o, \omega_3/\omega_o, t_3/T_o) &= (0.873, 0.31244, 10.54)\end{aligned} \tag{8}$$

Based on the tsunami wave generation theory, the velocity u_p of numerical wave paddle can be formulated as

$$u_p = \sum_{i=1}^{3} C_i\eta_i/(h + \eta_i) \tag{9}$$

In the calculation domain, the wave absorbing layer has been adopted at the outflow boundary by adding an artificial fraction factor. At the top of the computational domain, the atmospheric pressure is imposed. At both sides of the domain, the symmetric boundary is used and the wall boundary is set at the bottom.

Due to the hydrodynamic forces on the PLEM oscillate seriously under the tsunami-like wave, the Fast Fourier Transform (FFT) method is used to transfer the forces signals from time to frequency domain, which is helpful to analyze the power of the tsunami-like wave on the PLEMs. The FFT of non-periodic continuous-time force signal $F(t)$ can be expressed as [22]

$$P(\omega) = \int_{-\infty}^{\infty} F(t)e^{-j\omega t}d_t \tag{10}$$

where $F(t)$ is the force signals in time domain; $P(\omega)$ is the power signals in frequency domain; j is an imaginary number.

III. MODEL VALIDATIONS

A. WAVE PROFILES

The profiles of the solitary and tsunami-like waves are verified depending on the comparison between the analytical solutions and the numerical results. Wave height H and still water depth h which compose the total wave depth h_t are 2 m and 8 m, respectively. The length and height of the calculation domain are set as 1500 m and 20 m respectively, due to the long wavelength of the tsunami-like wave. The mesh consists of 380,132 cells and in the propagation region of the wave height, 40 mesh layers are used. The tsunami-like wave is generated by the numerical wave paddle at different times in Fig. 1. With the movement of the paddle, the water is compressed and the water level rises. Depending on the different movement velocities of the paddle, different waves can be generated. The predicted wave profiles are compared with analytical solutions as shown in Fig. 2, which depicts that the numerical data are in good agreement with analytical solutions. Besides, the duration and wavelength of tsunami-like wave are much longer than that of solitary wave. It implies that the energy contained in the tsunami-like wave is more than that of solitary wave.

B. WAVE FORCES

Solitary wave punching on the subsea pipeline is simulated to evaluate the calculation capability of this model. The corresponding experiment was carried out by Sibley [23]. The whole calculation domain is 40m in length and 0.5 m in height. The wave height H and water depth h are 0.034 m and 0.17 m, respectively, and the period of the wave is 0.99 s. The pipeline diameter is 0.034 m. From the pipeline

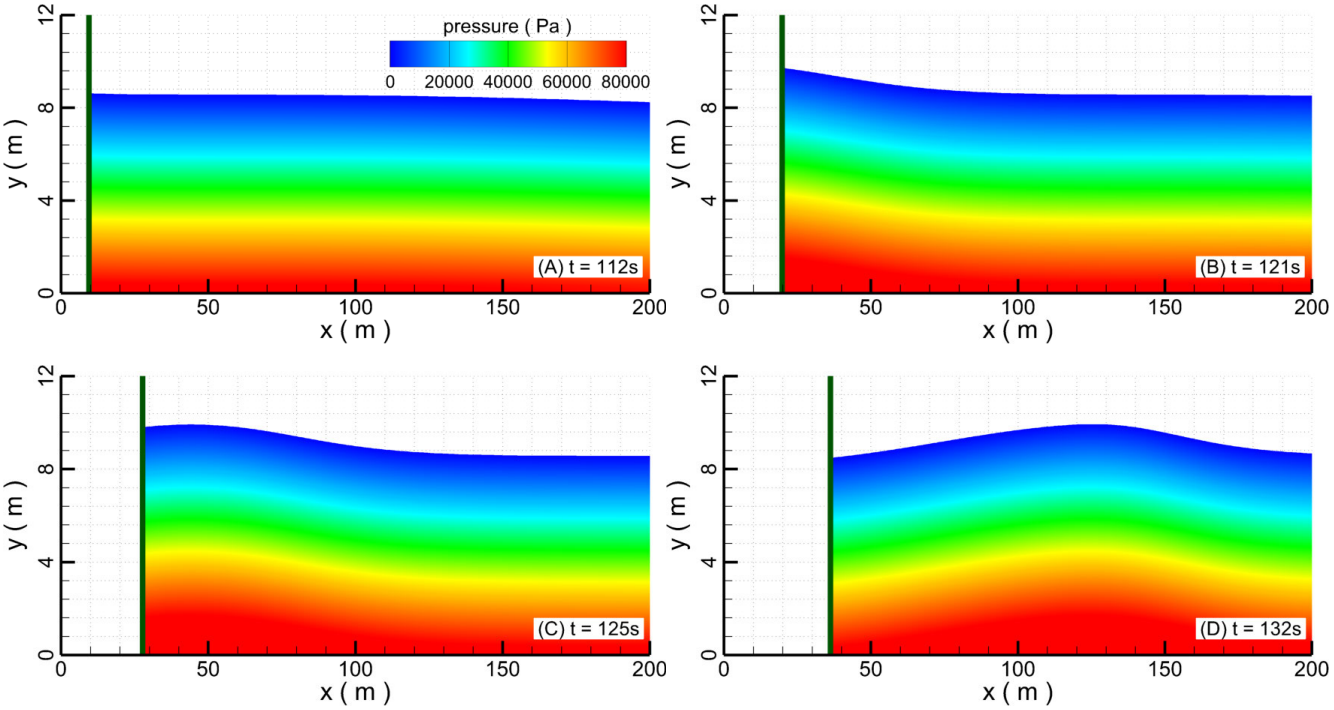

FIGURE 1. Tsunami-like wave generation at different times.

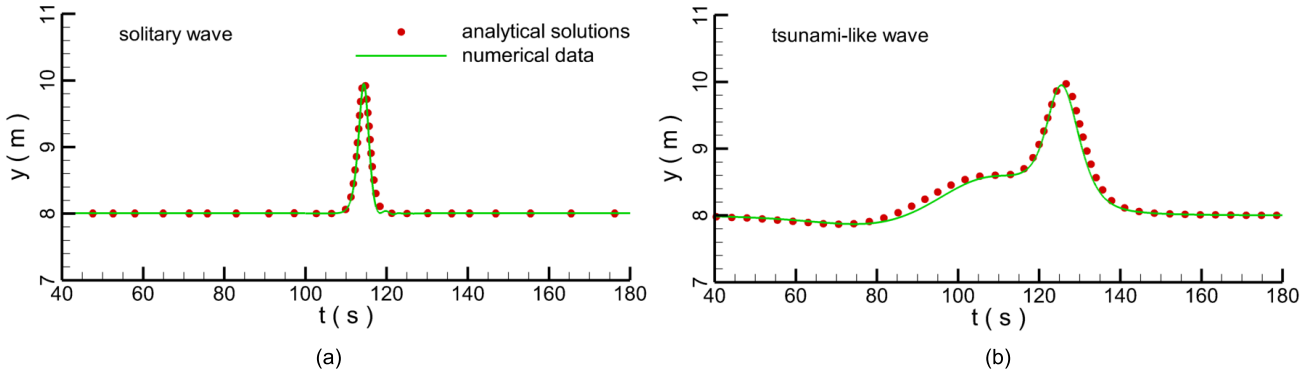

FIGURE 2. Comparison between the numerical data and analytical solutions.

center which is located at x = 3 m to the bottom, the distance is 0.0884 m. The whole mesh consists of 421,588 grids, and around the pipeline, the finest grid spacing is 0.05 mm. To ensure the calculation accuracy, a medium mesh (214,554 grids) and a coarse mesh (51,586 grids) are also generated for comparison. The calculation was performed on a Dell Precision 3630 Tower which includes 12 central processing units (CUPs). The CPU type is Intel (R) Core (TM) i7-8700 CUP @ 3.20GHz. The run times with the fine, medium and coarse meshes are 5, 12 and 25 h, respectively. The vorticity contours around the pipeline at different times are drawn in Fig. 3. When the solitary wave approaches the pipeline, the vortices are generated at t = 3.8 s. With the passing of the wave, the vortices gradually develop (t = 4.1 s) and grow (t = 4.4 s). Finally, these vortices shed from the pipeline after the wave passes the pipeline. The comparisons between the predicated hydrodynamic forces normalized by $\rho ghA(A = \pi D^2/4)$ and measured data are plotted in Fig. 4. The hydrodynamic forces denote pressure and shear stress. In the rest of the paper, all hydrodynamic forces are normalized using the same method. Forces for the dense and medium meshes which are in good agreement with corresponding measurements are nearly identical, whereas those computed on the coarse mesh are noticeably different from measurements. So, the resolution of dense mesh is sufficient. The computational capability of present model is well validated in predicting the wave profiles and hydrodynamic forces. Please refer to Qu *et al.* [24] for more details regarding this numerical model and its other validations.

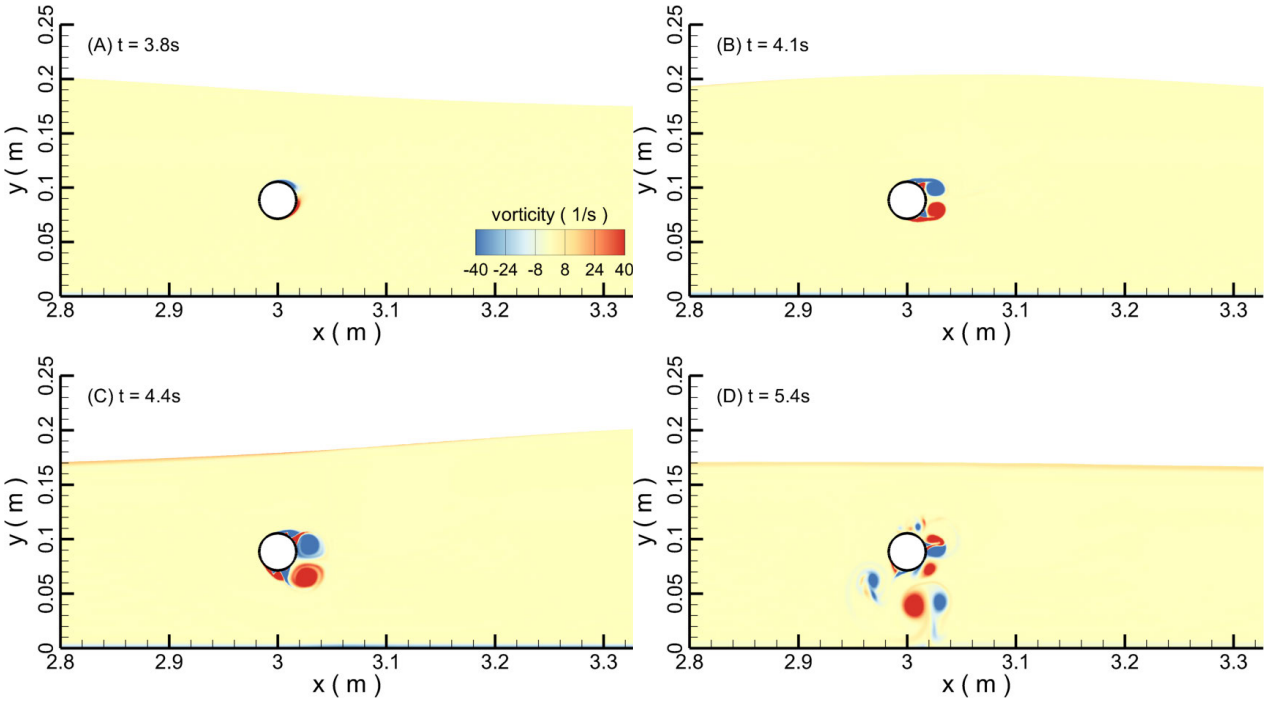

FIGURE 3. Vorticity contours at different times.

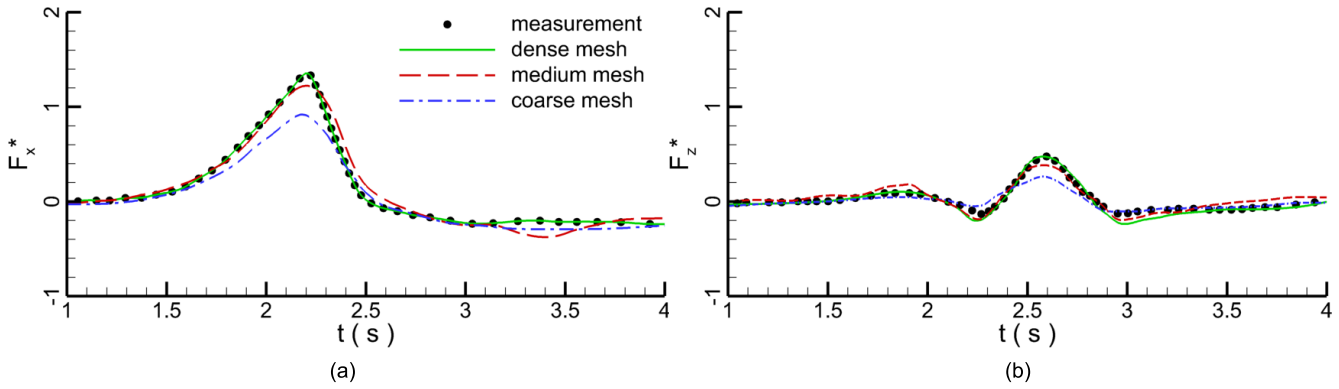

FIGURE 4. Hydrodynamic force comparisons between the numerical and experimental data; (a) horizontal force; (b) vertical force.

IV. RESULT AND DISCUSSION

The flow characteristics and hydrodynamic forces on PLEM after different tsunami-like waves impinging on various PLEMs consisted of upstream pipe (UP), downstream pipe (DP) and bottom seat (BS) are studied in the following sections. The length and height of calculation domain are 1500 m and 20 m, respectively. The origin of the coordinate system locates at left-bottom corner and the left side of PLEM is at the x = 80 m. The height (H_b) of the BS is 0.6 m and distance (S_a) from the center of the pipes (UP and DP) to the top of the BS is 0.4 m. The diameters (D) of the pipes are 0.8 m. The still wave depth (h) is kept as 8 m for all the calculations. Besides, H is wave height, L_b is the length of BS, and S is the distance between two centers of the pipes, as depicted in Fig. 5. The time series of water surface are recorded at the elevation sensors (A: x = 70 m and B: x = 100 m). Depending on the boundary layer theory and combining with the mesh scale in validation case, the finest mesh scale around the PLEM is 0.2 mm and the mesh is gradually stretched from working zone ($0 < x < 200$ m) with the scaling ratio of 1.2. The calculation meshes consist of 541,476 to 642,582 grids and 40 mesh layers are employed to resolve the propagation region of wave height.

A. FLOW PHENOMENA

In this section, the basic case simulation with wave height $H = 2$ m, distance $S = 2$ m and length $L_b = 10$m is carried out. When the wave enters the calculation domain, the wave profiles at sensor A and B are recorded, as shown in Fig. 6. Correspondingly, the moments of vorticity contours shown

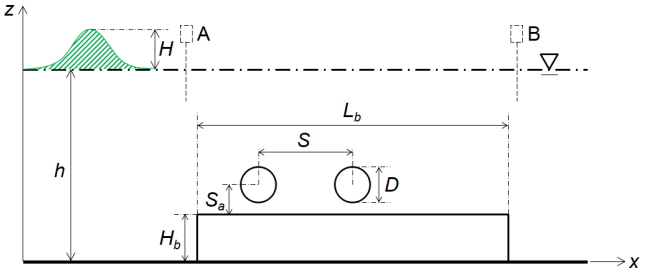

FIGURE 5. Schematic calculation domain for wave impacting PLEM.

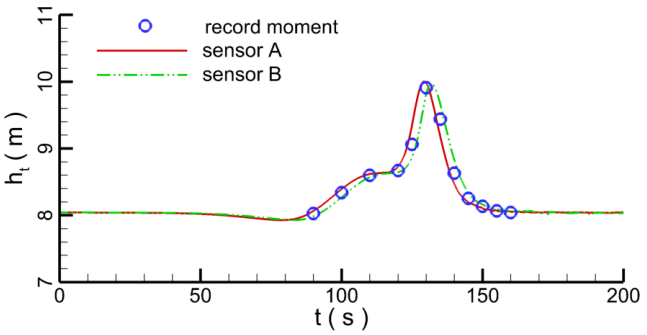

FIGURE 6. The wave profiles recorded at sensor A and B.

in Fig. 7 are signed in Fig. 6 with the blue circle. The flow field develops from a stationary state. With the generation of wave, when the leading-depression wave portion of tsunami-like wave arrives at the PLEM, the water level decreases inducing an upstream flow. A few weak detached vorticities are generated in front of every part of PLEM at 90 s. Then, the water level increases following the increment of wave at the preceding elevated wave portion, and the flow direction reverses to downstream. A few vorticities are produced behind the pipes (UP and DP) and at the corners of bottom seat (BC) due to the block effect of objects on the wave flow at 110 s. With the propagation of the wave, the water level continues to increase and the flow velocity increases, too. The vorticities become bigger and bigger, and are shed from the PLEM. The vorticities shed from the UP act on the DP where the combining vortices in different sizes and intensities appear from 110 s to 130 s. When the peak of wave at the secondary elevated wave portion is above the PLEM from 130 s to 135 s, the mutual interaction between the PLEM and the wave is the strongest and the flow oscillates severely in the vicinity of the PLEM. Due to the superposition of eddies generated by different parts of the PLEM, some irregular and intensity vorticities emerge above the BS. After the vorticities shed from the PLEM, a Karman vortex street forms at 130 s. By the time the tsunami-like wave passing over the PLEM, the vortices have dissipated but there are still many pairs of vorticities rotating in the flow due to the oscillation of the water. Finally, the vortices are distributed in the whole flow domain. Moreover, due to the wave energy dissipation by the PLEM, the waveform changes. The peak elevation at the rear side sensor B decreases about 3.4% compared with that recorded at the front side of the PLEM. In other words, although there is a strong interaction between the wave and PLEM, only little energy took by the wave is dissipated.

When the tsunami-like wave impinges the PLEM, the hydrodynamic horizontal and vertical forces on every part (UP, DP, and BS) of PLEM are recorded. Due to the leading-depression wave is weak, before the 80s, there have been little negative forces on the PLEM. With the increase of the water level and velocity, the forces on the PLEM increase. When the wave passes over the PLEM, the hydrodynamic horizontal forces on the pipes (UP and DP) oscillate severely as seen in Figs. 8a, because when the wave passes the PLEM, more vortices which act on the pipes are generated between the pipes due to the interaction between the wave and PLEM. The vortices are unstable and volatile, so the forces on the pipes vibrate intensely. However, the horizontal forces on the BS are relatively stable. Comparing with the pipes, the bottom seat (BS) mainly suffers the hydrodynamic horizontal forces under the flow and the vortices from the upstream to downstream causes little horizontal shear force on BS. In the vertical direction, every part of the PLEM oscillates strongly due to the effect of the shedding vortices (Fig. 8b). The amplitude of the vertical force on the BS is larger than on the pipes because the vortices shed from the pipes swap up and down causing larger stress on the top of the BS. Moreover, the duration of the forces on the BS is also much longer than other parts (UP and DP). In order to analyze the power of the tsunami-like wave on the PLEM and compare the effects of tsunami-like wave on different parts of PLEM, the Fast Fourier Transform (FFT) method is employed [25] and horizontal and vertical power spectrums about UP, DP and BS are shown in Figs. 9a and 9b. The energy in the low frequency range is higher for BS compared to UP and DP. Because comparing with the pipes (UP and DP), the scale of the BS is much larger which suffers more hydrodynamic forces. Besides, the lower the frequency is, the weaker the oscillation of force on the object is. The change of hydrodynamic horizontal force on the BS is moderate so that the power on the BS reduces rapidly to the zero with the increase of frequency. However, the power on the pipes exists in different frequency due to the violent oscillation of the forces. This indicates that although the hydrodynamic forces on the pipes (UP and DP) are smaller than that of the BS, vortices shed from the pipes cause serious impact on the vibration of the pipes. Besides, the vertical force on the BS oscillates more serious than the horizontal force because the shedding vortices generated above the BS are applied on the upper surface of BS and cause the change of the vertical force. Overall, due to the complex structure of the PLEM, under the tsunami-like wave, every part of the PLEM suffers serious hydrodynamic loads and receive the impact of the shedding vortices. The phenomena are harmful to the PLEM.

B. EFFECT OF WAVE HEIGHT ON PLEM

In the marine environment, the effects of waves with different heights on the marine infrastructures are significantly

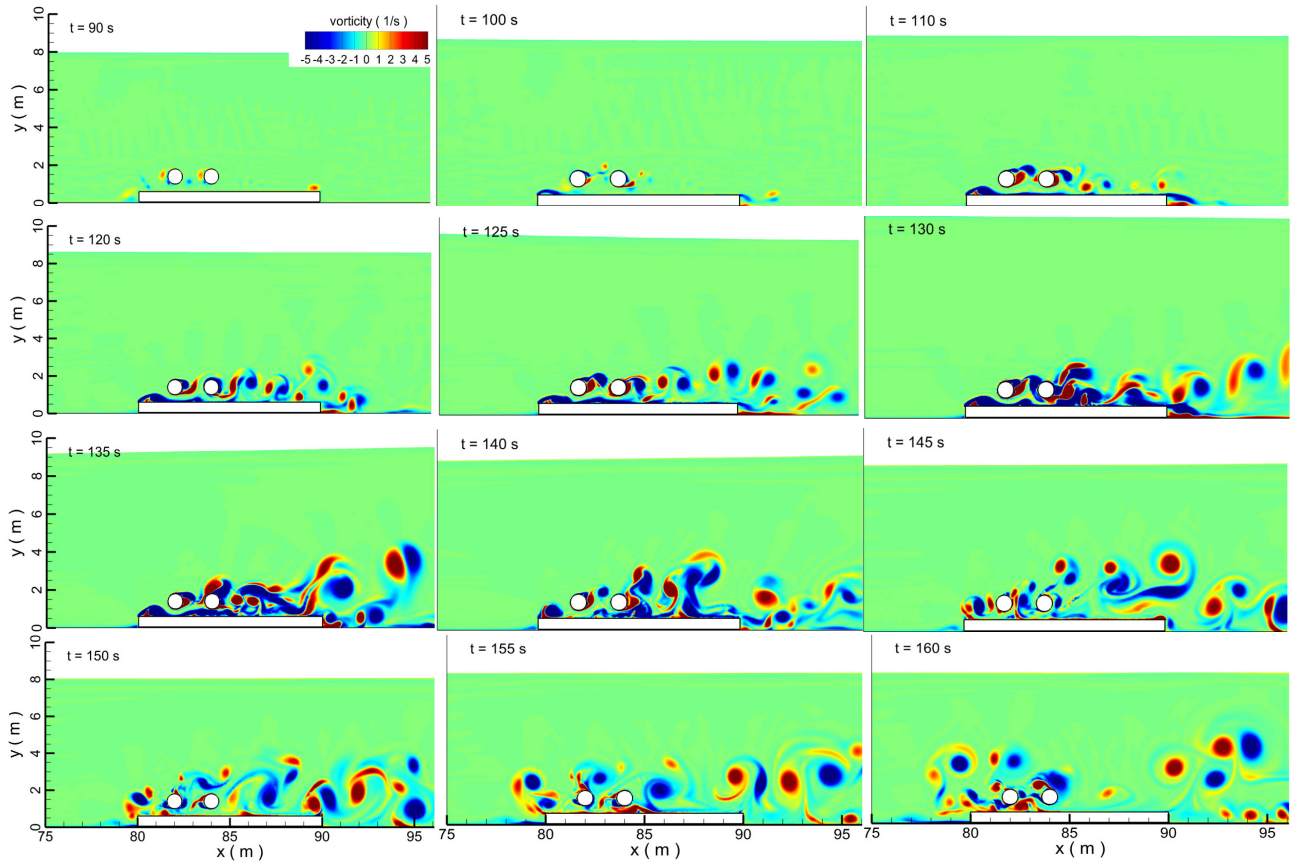

FIGURE 7. Snapshots of vorticity contours at different time instances.

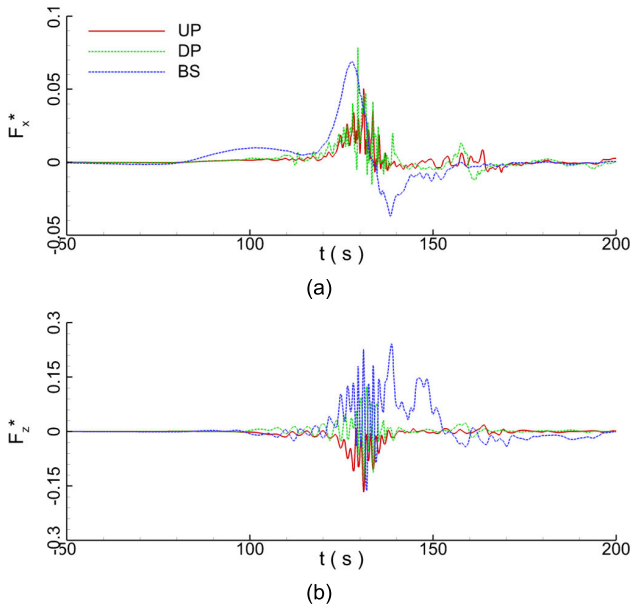

FIGURE 8. Forces on the PLEM in the temporal domain; (a) horizontal force; (b) vertical force.

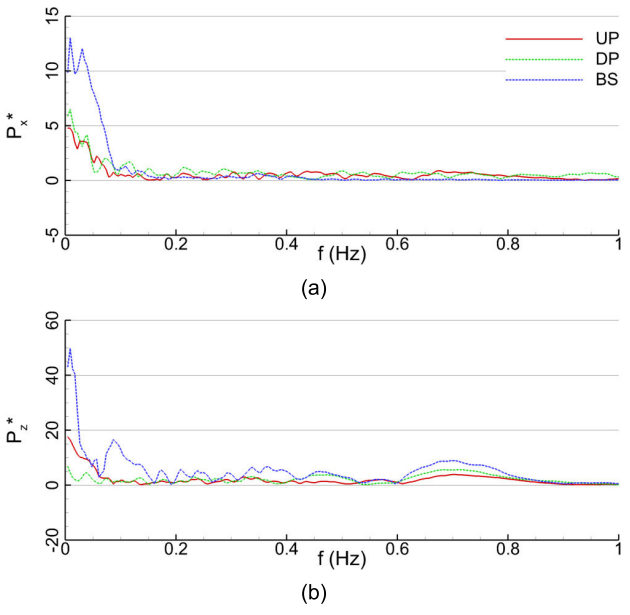

FIGURE 9. Power on the PLEM in the frequency domain; (a) horizontal power; (b) vertical power.

different. So, in this study, beside the wave height of 2 m, the various tsunami-like waves with heights of 1, 1.5, 2.5 and 3.0 m are also considered and the comparison of wave profiles is shown in Fig. 10. The two moments at the peaks of the preceding and secondary elevated wave parts are marked in the wave profiles, correspondingly, the snapshots of

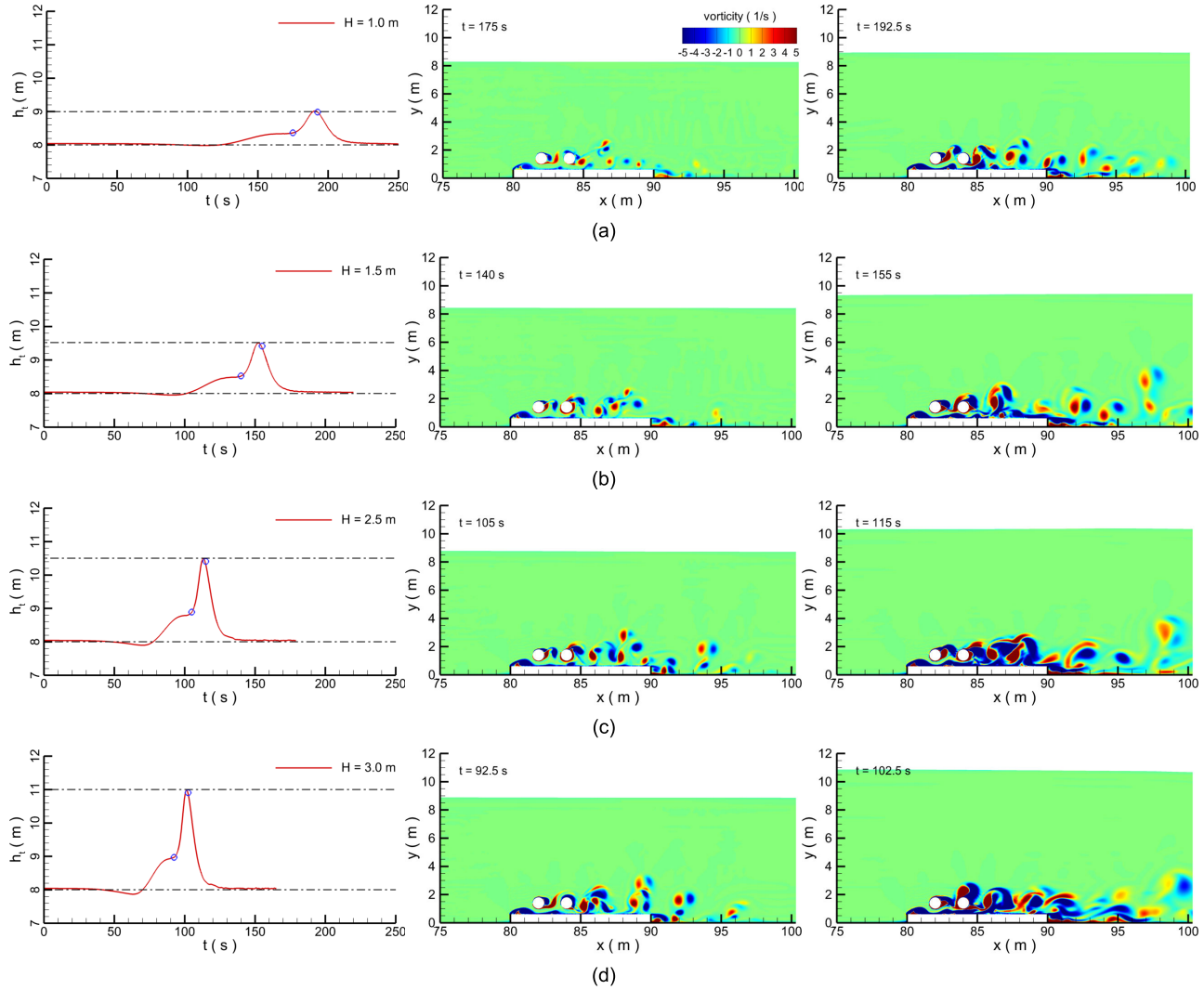

FIGURE 10. Wave profiles and corresponding vorticity contours at different wave heights; (a) $H = 1$ m; (b) $H = 1.5$ m; (c) $H = 2.5$ m; (d) $H = 3$ m.

vorticity contours at these two moments are following the wave profiles. Comparing with the wave profiles, with the increase of wave height, the change of wave profile at different wave height conforms to the law of tsunami wave propagation. When the tsunami wave is under shoaling, the wave height increases but the wavelength decreases. When the preceding elevated wave arrives at the PLEM, a few vortices shed from the UP, DP and BS, respectively. However, when the secondary elevated wave approaches the PLEM, more vortices are being shed and the vorticity is larger than that under the preceding elevated wave because the velocity and flux around the PLEM under the secondary elevated wave is larger than preceding elevated wave. Besides, when the vortices break away from PLEM, they combine together and some big vortices are generated. With the increase of the wave height, both the number of the vortices and vorticity increase, and the interaction between the vortices and PLEM is enhanced.

It is seen that the flow fields under different wave heights change severely, resulting in dramatically varying hydrodynamic loads. The maximum forces on every part of PLEM under different wave heights are depicted in Fig. 11. With the increase of the wave height, the horizontal forces on upstream pipeline UP and bottom seat BS increase linearly. However, the fluctuation of horizontal forces on the downstream pipe DP is not regular. Because with the increase of the wave height, the velocity also increases, the flow interacts with the UP and BS directly. The more the velocity is, the larger the hydrodynamic forces on the UP and BS are. Due to the block of the UP on the DP, the flow velocity reduces before it arrives at the DP and the forces caused by the unidirectional flow reduce, but the vortices shed from the UP impinge on the DP directly. The combination of the flow and vortices cause the significant oscillation of the hydrodynamic forces on the DP. So when the wave height changes from 1 m to 2.5m, the hydrodynamic forces on the DP increases. When the wave

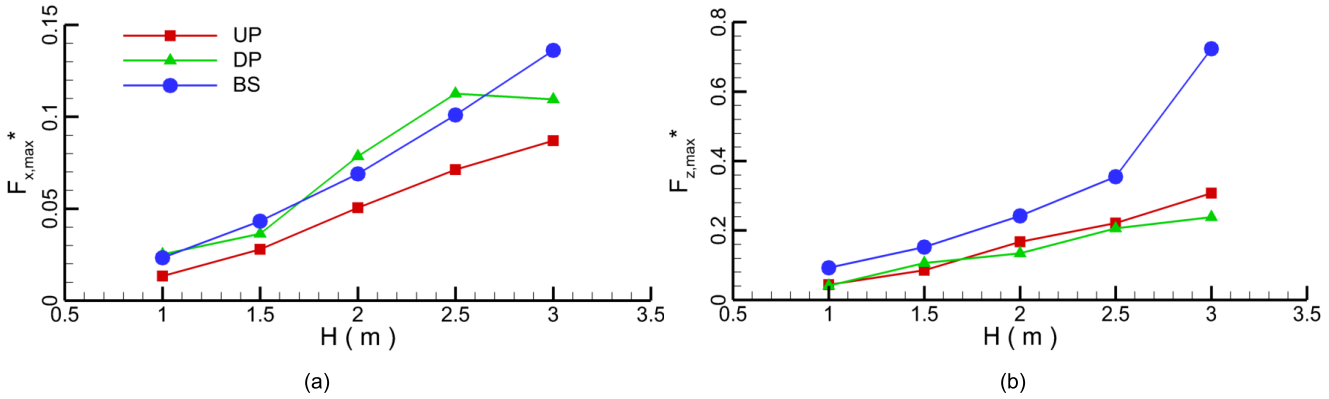

FIGURE 11. The maximum hydrodynamic forces on the PLEM under different wave heights; (a) horizontal forces; (b) vertical forces.

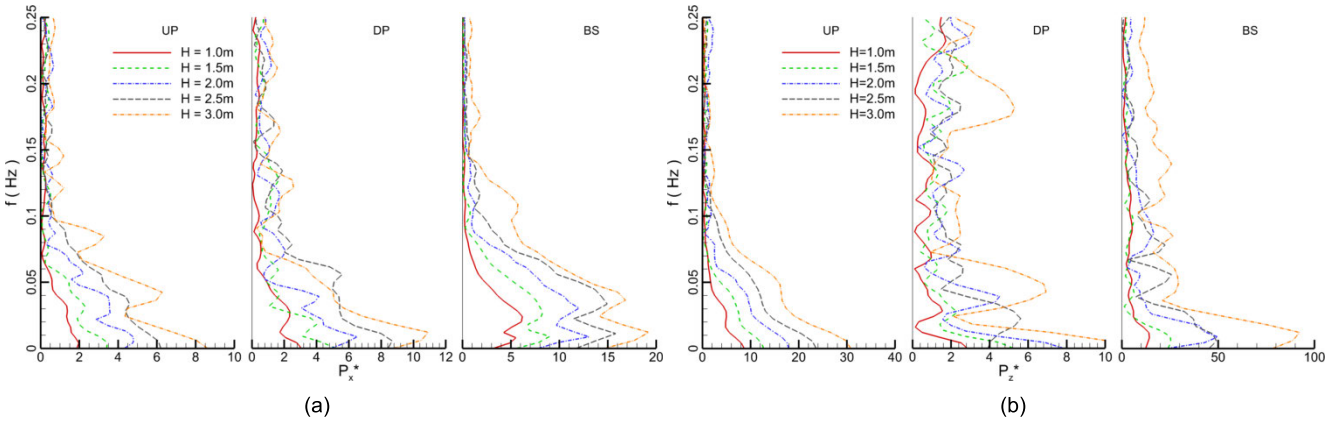

FIGURE 12. The power spectrum of PLEM under different wave heights; (a) horizontal hydrodynamic forces; (b) vertical hydrodynamic forces.

height is over the 2.5 m, the forces reduce slightly. With the increase of the wave height, the vertical hydrodynamic forces on every part of the PLEM increases. At the same case, the vertical forces on the BS are more than that of the UP and DP on which the forces are similar to each other.

During the processing of the tsunami-like wave propagation, the hydrodynamic forces on the PLEM oscillate severely which have been transferred to the power spectrum using FFT in Fig. 12. When the frequency is near to the zero, the horizontal power on the UP at different wave heights is bigger than other frequencies, which means that the change of hydrodynamic forces on the UP is smooth and the oscillation of the forces is weak. However, when the horizontal power on the DP and BS reaches the maximum, the frequency is more than that of UP, because the vortices shed from the UP have important effects on the DP and the oscillation frequency of the forces increase. Besides, it is found that with the increase of the wave height, the energy took by the tsunami increase and the power of the tsunami-like wave on the PLEM also increase. Comparing with the pipes (UP and DP), the power on the BS is the largest because the bigger the object is, the more serious the effects of the flow and vortices are. With the increase of the frequency, the power on the PLEM reduces gradually because when the frequency is over the oscillation frequency of forces on PLEM, the power on PLEM is over the limit range of the energy. In other words, the effect of high frequency oscillation force on pipeline is weak. As for the vertical power on the PLEM, due to the serious effect of the vortices, the power on the DP vibrates strongly inducing the DP is easily damaged because of fatigue failure.

C. EFFECT OF WAVE ON DIFFERENT PLEMS

In the marine engineering system, many PLEMs with different structure forms exist in submarine oil and gas fields. In order to investigate the effects of tsunami-like wave on different PLEMs, the change factors of PLEM which are the different distance between two pipes (UP and DP) and the length of bottom seat (BS) are considered in this section. In the study, the wave height H and still water depth h are 2 m and 8 m, respectively.

1) DISTANCE BETWEEN UP AND DP

The impacts of the center distance (S) between upstream pipe (UP) and downstream pipe (DP) on the hydrodynamics around PLEM have been numerically investigated.

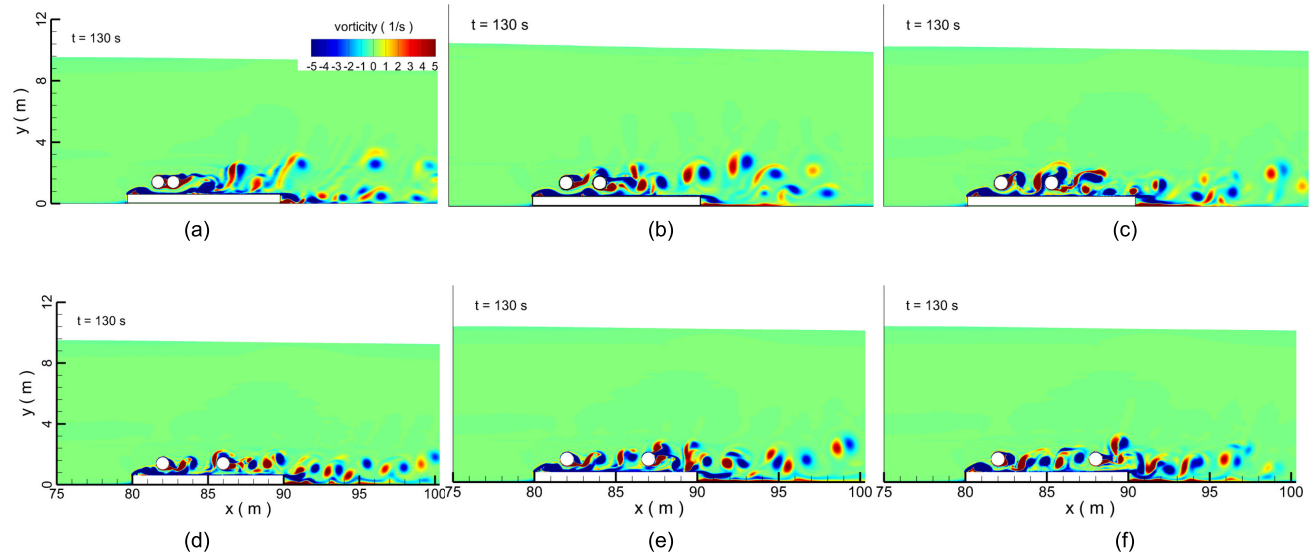

FIGURE 13. Snapshots of vorticity contours at different distances; (a) $S = 1.25D$; (b) $S = 2.5D$; (c) $S = 3.75D$; (d) $S = 5D$; (e) $S = 6.25D$; (f) $S = 7.5D$.

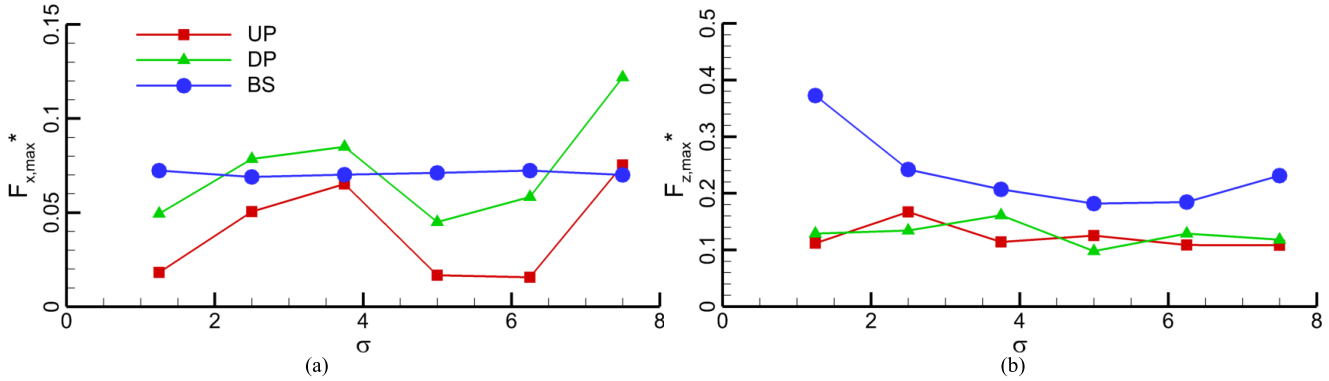

FIGURE 14. The maximum hydrodynamic forces on the PLEM with different distances; (a) horizontal forces; (b) vertical forces.

Six different distances are chosen, $S = 1.25D$, $2.5D$, $3.75D$, $5D$, $6.25D$ and $7.5D$. Fig. 13 shows the vorticity contours with different distances when the maximum water elevation is above the PLEM. When the distance S is $1.25D$, the gap between two pipes is so small that the vortices are trapped in the gap. Due to the block of vortices in the gap, the velocity before the DP is very small. The vortices shed from DP are very weak and quickly fade. When the distance S is $2.5D$, the length of the shedding vortices is just equal to the distance of the gap between two pipes, which means that the eddies just break away from the upstream pipeline (UP) and then touch the downstream pipe (DP). Comparing with vorticity contour with $S = 1.25D$, the number of vortices and the intensity of vorticity increase and more vortices shed from PLEM. When distance S increases more than $2.5D$, some pairs of vortices in the gap between two pipes can be seen clearly in Fig. 13. The vortices shed from UP cause the oscillation of flow around the DP and impact on the DP directly. The vortices break down after they impinge the DP. Behind the DP, the vortices are generated again due to the oscillation of the flow. Especially, at $S = 5D$, the vortices behind the DP shed periodically and the flow phenomena of Kármán vortex street are formed. When the distance S is $7.5D$, some pairs of vortices behind the UP appear obviously between two pipes (UP and DP), because the distance S is so long that the vortices can develop enough. Moreover, in every case, a pair of vortices behind the BS is generated due to the backflow. When distance S is longer than $2.5D$ and the vortices behind the DP arrive at the back end of the BS, the combination of vortices from pipes and BS shed from PLEM. The longer the distance S is, the larger the intensity of the vortices behind the DP is and the bigger the combination vortices behind the PLEM are. In general, the tsunami-like wave can induce a series of vortices shedding from the PLEM during its long wave duration. The vortices in the gap have important effects the DP. With the increase of the distance S, the effects of the vortices on every part of PLEM are enhanced.

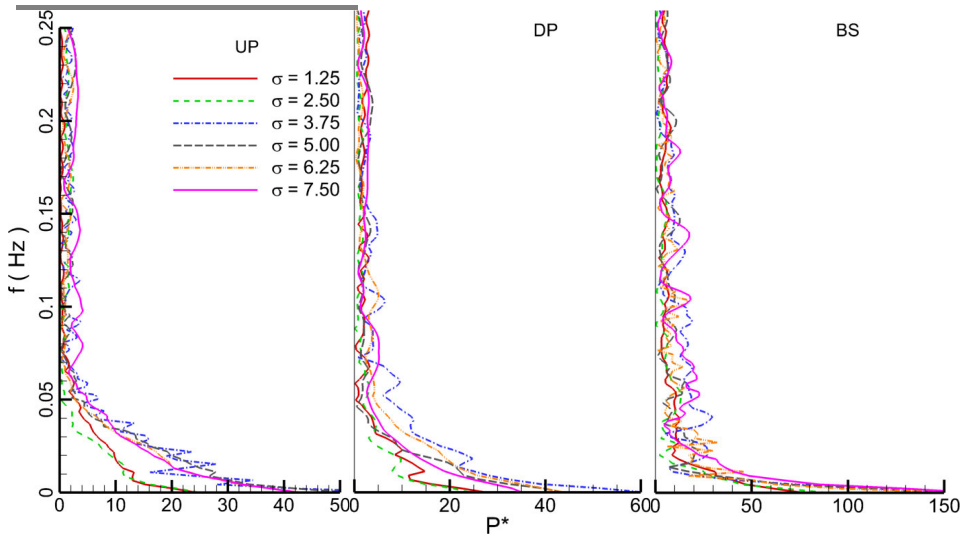

FIGURE 15. The power spectrum of PLEM with different distances for hydrodynamic forces.

Although the external environmental conditions of still water depth and wave height are unchanged, the hydrodynamic forces on the different PLEMs change seriously because of the change of the structure. The maximum hydrodynamic forces on the UP, DP and BS in horizontal and vertical directions are depicted in Fig. 14 in which the ratio σ is of the distance S to the pipeline diameter D. With the distance increase, the hydrodynamic horizontal force on the BS is unchanged. It is deduced that the change of the upper structure of the PLEM has little influence on the bottom structure. However, due to the strong influence of the vortices on the pipes, the maximum horizontal forces on the pipes change ups and downs. There are two explanations for these phenomena. Firstly, due to the block of UP, the flow velocity reduces before the flow arrives at the DP. The smaller the distance is, the greater the impact of flow on the DP. Secondly, the vortices shed from UP with different frequencies and strength impinge on the DP under different distances. When the distance is very small, the vortices without strength decay have strong impacts on the DP. Moreover, When the vortex shedding frequency from UP is similar to that from the DP, the resonance also causes the increase of the forces. Therefore, due to various influence factors, the horizontal forces on the PLEM are very unstable. With the increase of the distance, the fluctuation amplitude of vertical forces on the UP and DP is rather small but the vertical forces on the BS reduce slightly. Fig. 15 shows the power spectrum for the total hydrodynamic forces. When the ratio σ is less than 2.5, the power on the PLEM is less than other cases. When the ratio σ is 3.75, the power on the UP vibrate severely following the change of the frequency, which is indicated that the vortices shed from UP are extremely irregular. Compared with the UP and DP, the power on the BS is the largest and the oscillation of the forces is the most serious.

2) LENGTH OF BS

In order to analyze the hydrodynamic characteristics of PLEMs with different lengths under the tsunami-like wave, five lengths of PLEM bottom seat are selected as $L_b = 6.25D$, $7.5D$, $8.75D$, $10D$, $11.25D$ and $12.5D$. The vorticity contours at different lengths under the tsunami-like wave are shown in Fig. 16. When the preceding elevated wave peak is above the PELM, only a few pairs of the shedding vortices are generated behind the pipes and BS due to the low velocity of flow. Even so, at the short BS, the interference effects among the vortices shed from DP and BS are significant and the rotation direction of the vortices change. When the secondary elevated wave peak approaches the PLEM, many strong vortices shed from every part of the PLEM. When the length of BS is very short, it is extremely difficult to distinguish which part of the PLEM these vortices come from. Because the vortices shed from DP exhibit strong mutual interaction with the whirlpools behind the BS badly, and they combine together and shed from the PLEM irregularly. With the increase of the PLEM length, the interaction between different vortices is weakened. When the length L_b is $10D$, a Kármán vortex street is generated behind the pipes and a pair of the attachment vortices are behind the BS. Once the length increases to $12.5D$, the vortices behind the pipes and BS do not interact with each other. In conclusion, although the flow fields are different at various BSs, the length of the BS does not have a significant impact on the flow field due to two reasons. Firstly, the flow velocity is very low around the BS which is on the seabed. Secondly, the pipes above the BS have disturbed the flow seriously before the water flows from the front to the rear of the BS, which can reduce the pressure difference around the BS.

However, although the flow fields are not changed significantly, it is necessary to investigate whether the change of the BS shape has significant effects on the hydrodynamic

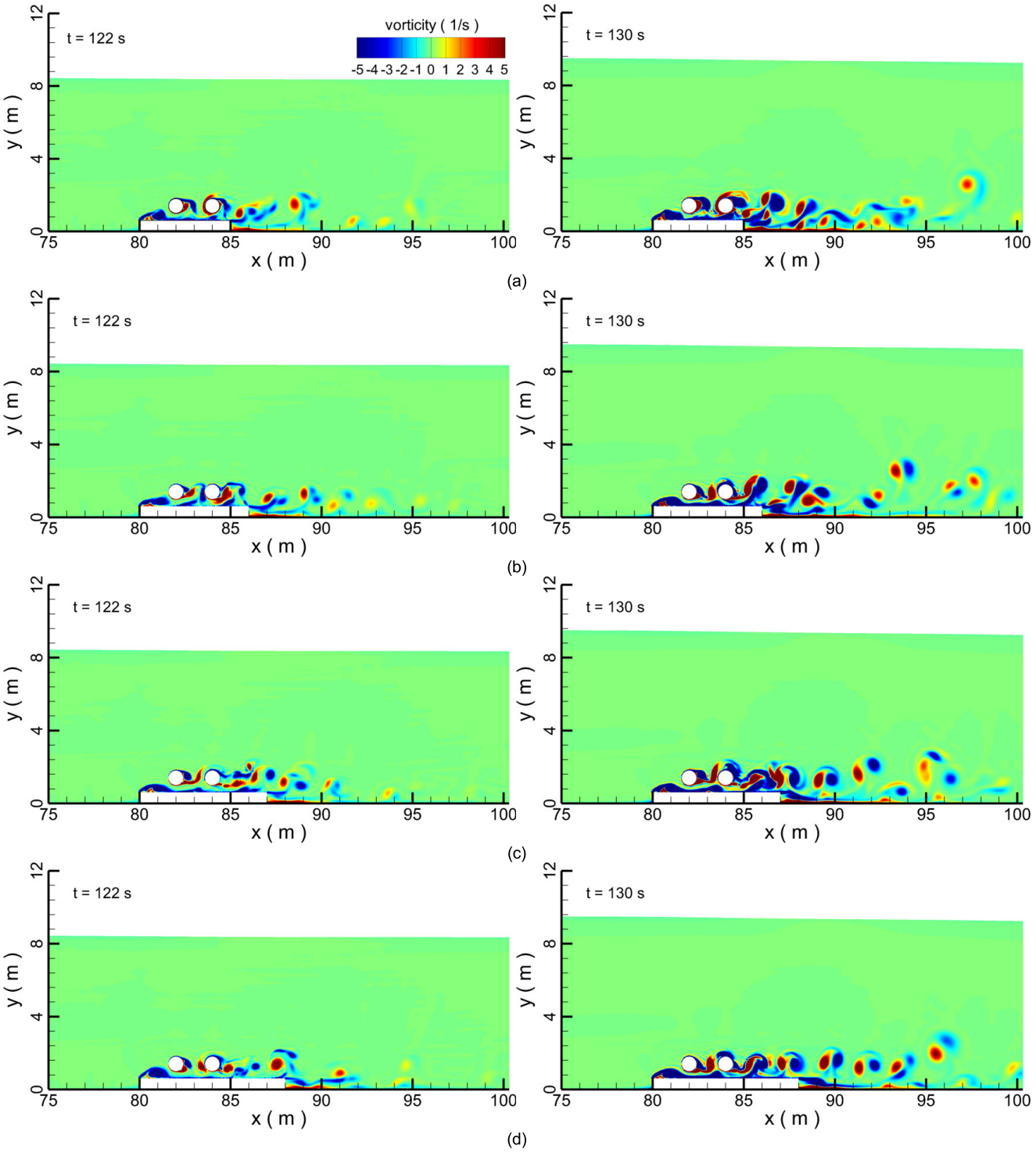

FIGURE 16. Snapshots of vorticity contours at different BS lengths; (a) $\lambda = 6.25$; (b) $\lambda = 7.5$; (c) $\lambda = 8.75$; (d) $\lambda = 10$.

forces on the PLEM or not. The hydrodynamic forces on the PLEM are recorded and the maximum hydrodynamic forces are depicted in Fig. 17 where the ratio λ is of the BS length L_b to the pipe diameter D. In the horizontal direction, with the increase of the BS length, the hydrostatic forces increase but the hydrodynamic forces on the UP and BS changes weakly. The hydrodynamic horizontal forces on the DP are larger than that of the UP and BS. Especially, when the ratio of the BS length to the pipe diameter is 10, the frequencies of the shedding vortices from UP and DP are similar causing the resonance phenomenon of DP, so the horizontal hydrodynamic force on the DP at ratio of 10 is the largest than other

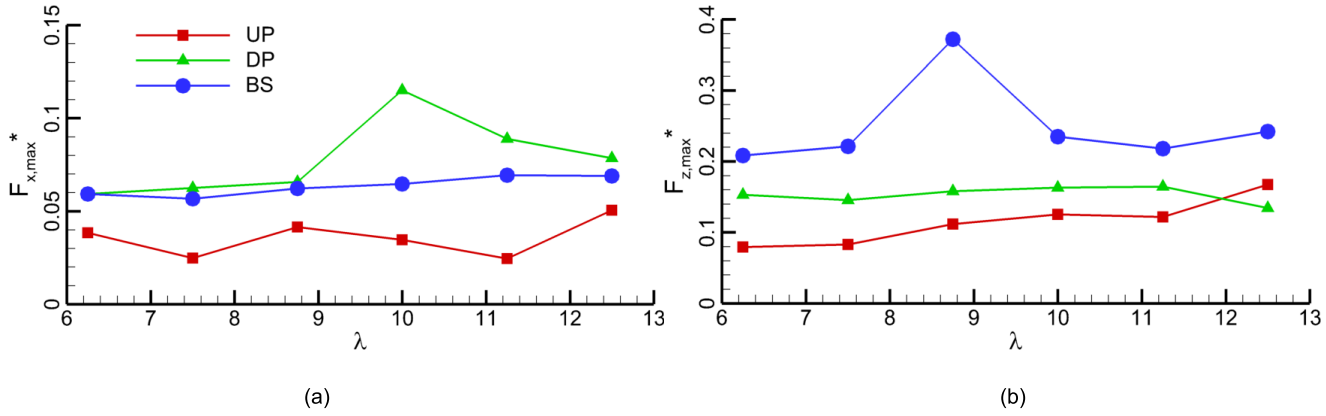

FIGURE 17. The maximum hydrodynamic forces on PLEM with different BS lengths; (a) horizontal force; (b) vertical force.

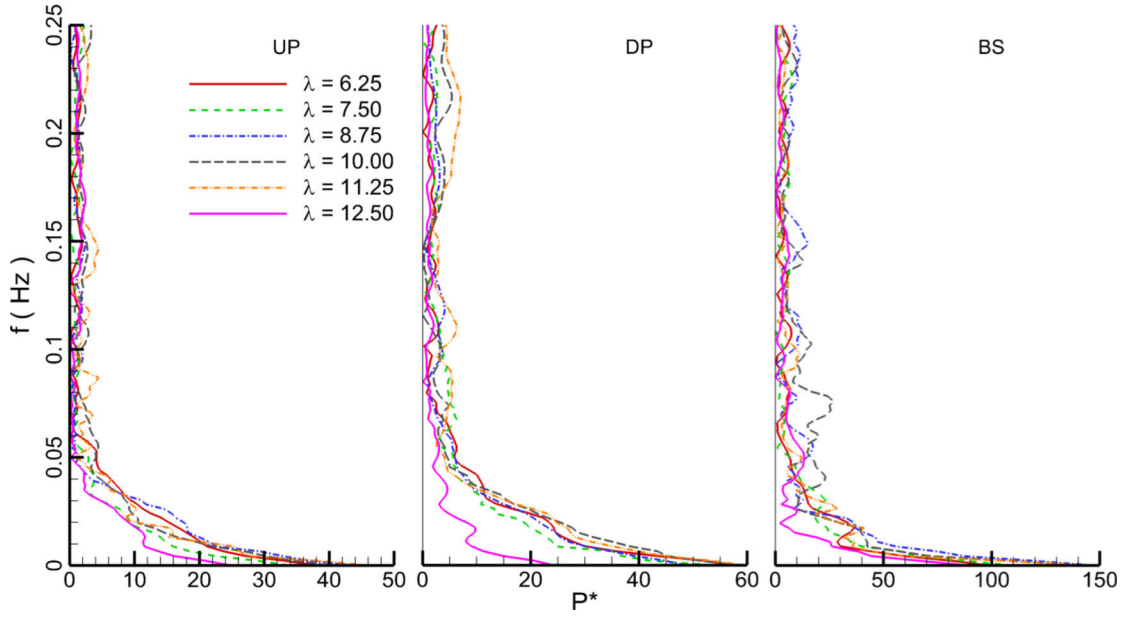

FIGURE 18. The power spectrum of PLEM with different BS lengths for hydrodynamic forces.

cases. As for the vertical hydrodynamic forces, at the same BS length, the force on the BS is larger than that of UP and DP. When the ratio is 9, the hydrodynamic vertical force on the BS is the largest because of the serious effect of combination vortices from UP and DP on the BS. The change of the UP and DP is very small with the increase of BS length. The power spectrum for the total hydrodynamic forces is depicted in Fig. 18. When the ratio is 12.5, the power on every part of the PLEMs is less than that under other ratios. The longer the BS, the lower the power on the PLEMs. The big bottom seat (BS) can provide strong support for the PLEM. In other words, compared with the UP and DP, the power on the BS is the largest. Besides, due to the effect of vortices on the PLEM, the forces on the PLEMs oscillate and the power exists at different frequencies.

V. CONCLUSION

In this paper, the attack of tsunami-like waves on the Submarine Pipeline End Manifolds (PLEM) is investigated depending on our numerical model. The effects of wave height, distance between two pipes (UP and DP) and length of bottom seat (BS) on the hydrodynamic forces of PLEM are studied. Depending on the FFT method, the power on every part of PLEM is also analyzed under different conditions. The main conclusions drawn from the investigation can be summarized as follows: (1) With the propagation of the tsunami-like wave and the increase of the wave level, more and more vortices behind every part of PLEMs are generated and they combine together interacting with the PLEMs. When the secondary elevated wave peak is above the PLEM, the mutual interaction between the PLEM and

the wave is the strongest and the vortices vibrate severely around the PLEM. Due to the effects of the vortices on the PLEM, the hydrodynamic forces on the PLEM also oscillate strongly. In the power spectrum, it is observed that the force and power on the BS are bigger than other parts of the PLEM, however, the oscillation frequency of the BS is lowest, which means that BS is easy to be damaged by the flow but the vortices cause little effect on the BS. Comparing with the BS, the vortices are more harmful to the pipes (UP and DP). (2) With the increase of wave height, the interaction between the vortices and the PLEMs are enhanced and both the number of vortices and vorticity increase. Besides, the higher the wave is, the larger the velocity of the wave is. The maximum hydrodynamic forces on the UP and BS increase monotonously with wave height, however, due to the strong influence of the vortices shed from UP on DP, the maximum hydrodynamic forces on the DP increase when the wave height is less than 2.5 m, then the forces reduce slightly when the wave height is over 2.5 m. (3) When the structure of the PLEM changes, the distance between the pipes has some influence on the maximum hydrodynamic forces on the PLEM, and the vortices shed from PLEM are also different. When the distance between the two pipes is very small, a pair of vortices exist in the gap and connect two pipes. With the increase of the distance, vortices cause strong mutual interactions between UP and DP. If the length of the BS changes, when the length of BS is very short, it is extremely difficult to distinguish which part of the PLEM these vortices come from because vortices from different PLEM parts combine together and shed from PLEM irregularly. When the length L_b is $10D$ and wave peak approaches the PLEM, a Kármán vortex street is generated behind the pipes and a pair of the attachment vortices are behind the BS. The simulation results indicate that comparing with the pipes, the power and forces on the bottom seat are the largest which is easily damaged if the forces on the BS are larger than ultimate stresses. However, the pipes which are affected seriously by the vortices are vulnerable to fatigue failure. Overall, it is believed that the findings drawn from this work could enhance our understanding of the interaction between tsunami wave and marine engineering.

REFERENCES

[1] H. Kanamori, "Mechanism of tsunami earthquakes," *Phys. Earth Planet. Interiors*, vol. 6, no. 5, p. 359, 1972.
[2] V. Titov, F. Gonzalez, H. Mofjeld, and J. Newman, "Real-time tsunami forecasting: Challenges and solutions," *Natural Hazards*, vol. 35, no. 1, pp. 35–41, 2005.
[3] S. Anawat, K. Shunichi, I. Kentaro, M. Erick, G. Hideomi, M. Abdul, and I. FumihikO, "Damage characteristic and field survey of the 2011 great east Japan tsunami in miyagi prefecture," *Coastal Eng. J.*, vol. 54, no. 1, 2012, Art. no. 1250005.
[4] M. Heidarzadeh, A. Muhari, and A. B. Wijanarto, "Insights on the source of the 28 September 2018 sulawesi tsunami, Indonesia based on spectral analyses and numerical simulations," *Pure Appl. Geophys.*, vol. 176, pp. 25–43, Dec. 2018.
[5] P. S. Putra, A. Aswan, K. A. Maryunani, E. Yulianto, and W. Kongko, "Field survey of the 2018 sulawesi tsunami deposits," *Pure Appl. Geophys.*, vol. 178, pp. 2203–2213, Apr. 2019.
[6] Í. Aniel-Quiroga, C. Vidal, J. L. Lara, M. González, and Á. Sainz, "Stability of rubble-mound breakwaters under tsunami first impact and overflow based on laboratory experiments," *Coastal Eng.*, vol. 135, pp. 39–54, May 2018.
[7] T. Ha, J. Shim, P. Lin, and Y.-S. Cho, "Three-dimensional numerical simulation of solitary wave run-up using the IB method," *Coastal Eng.*, vol. 84, pp. 38–55, Feb. 2014.
[8] M. Maza, J. L. Lara, and I. J. Losada, "Tsunami wave interaction with mangrove forests: A 3-D numerical approach," *Coastal Eng.*, vol. 98, pp. 33–54, Feb. 2015.
[9] P. A. Madsen, D. R. Fuhrman, and H. A. Schäffer, "On the solitary wave paradigm for tsunamis," *J. Geophys. Res.*, vol. 113, pp. 286–292, Dec. 2008.
[10] G. Chen and R. Liu, "Upper bound solutions of vertical bearing capacity of skirted mudmat in sand," *Appl. Ocean Res.*, vol. 73, pp. 100–106, Apr. 2018.
[11] Y. Wang, H. Zhao, D. Wang, M. Xu, M. I. Lourenco, and S. F. Estefen, "Modeling for the optimization evaluation of layout scenarios of subsea cluster manifolds considering three connection types," *Marine Technol. Soc. J.*, vol. 48, no. 6, pp. 98–111, 2014.
[12] B. W. Nam, N. W. Kim, and S. Y. Hong, "Experimental and numerical study on coupled motion responses of a floating crane vessel and a lifted subsea manifold in deep water," *Int. J. Nav. Archit. Ocean Eng.*, vol. 9, pp. 552–567, Jan. 2017.
[13] Y. Wang, H. Tuo, L. Li, Y. Zhao, H. Qin, and C. An, "Dynamic simulation of installation of the subsea cluster manifold by drilling pipe in deep water based on OrcaFlex," *J. Petroleum Sci. Eng.*, vol. 163, pp. 67–78, Apr. 2018.
[14] Y. T. Wu, C. L. Yeh, and S. C. Hsiao, "Three-dimensional numerical simulation on the interaction of solitary waves and porous breakwaters," *Coastal Eng.*, vol. 85, pp. 12–29, Mar. 2014.
[15] E. Zhao, B. Shi, K. Qu, W. Dong, and J. Zhang, "Experimental and numerical investigation of local scour around submarine piggyback pipeline under steady current," *J. Ocean Univ. China*, vol. 17, no. 2, pp. 244–256, 2018.
[16] I. C. Chan and P. L. F. Liu, "On the run-up of long waves on a plane beach," *J. Geophys. Res.*, vol. 117, no. C8, pp. 72–82, 2012.
[17] K. Qu, X. Y. Ren, S. Kraatz, and E. J. Zhao, "Numerical analysis of tsunami-like wave impact on horizontal cylinders," *Ocean Eng.*, vol. 145, pp. 316–333, Nov. 2017.
[18] K. Qu, W. Y. Sun, H. S. Tang, C. B. Jiang, and J. Chen, "Numerical study on hydrodynamic load of real-world tsunami wave at highway bridge deck using a coupled modeling system," *Ocean Eng.*, to be published.
[19] E. J. Zhao, K. Qu, and L. Mu, "Numerical study of morphological response of the sandy bed after tsunami-like wave overtopping an impermeable seawall," *Ocean Eng.*, vol. 186, Jun. 2019, Art. no. 106076.
[20] E. J. Zhao, J. K. Sun, H. Jiang, and L. Mu, "Numerical study on the hydrodynamic characteristics and responses of moored floating marine cylinders under real-world tsunami-like waves," *IEEE Access*, vol. 7, pp. 122435–122458, 2019.
[21] E. J. Zhao, K. Qu, L. Mu, S. Kraatz, and B. Shi, "Numerical study on the hydrodynamic characteristics of submarine pipelines under the impact of real-world tsunami-like waves," *Water*, vol. 11, no. 2, p. 221, 2019.
[22] J. W. Cooley and J. W. Tukey, "An algorithm for the machine calculation of complex Fourier series," *Math. Comput.*, vol. 19, pp. 279–301, Jan. 1965.
[23] P. O. Sibley, "The solitary wave and the forces it imposes on a submerged horizontal circular cylinder: An analytical and experimental study," Ph.D. dissertation, City Univ. London, London, U.K., Sep. 1991, pp. 1–288.
[24] K. Qu, X. Y. Ren, and S. Kraatz, "Numerical investigation of tsunami-like wave hydrodynamic characteristics and its comparison with solitary wave," *Appl. Ocean Res.*, vol. 63, pp. 36–48, Feb. 2017.
[25] B. S. Reddy and B. N. Chatterji, "An FFT-based technique for translation, rotation, and scale-invariant image registration," *IEEE Trans. Image Process.*, vol. 5, no. 8, pp. 1266–1271, Aug. 1996.

ENJIN ZHAO received the B.S. and Ph.D. degrees from the College of Engineering, Ocean University of China, Qingdao, China, in 2012 and 2017, respectively.

He is currently with the College of Marine Science and Technology, China University of Geosciences, Wuhan, China. His research interests include ocean engineering and marine technology depending on the intelligent prediction of deep learning.

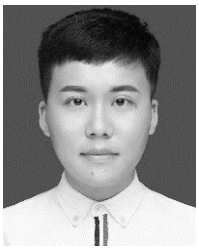

YUEZHAO TANG received the B.S. degree in science in geography from the China University of Geosciences, Wuhan, China, in 2019, where he is currently pursuing the M.S. degree in geological engineering. His research focuses on oil spill and maritime search-and-rescue depending on the intelligent prediction of deep learning.

JIE SHAO received the B.S. degree in harbor, waterway, and coastal engineering and the M.S. degree in harbor, coastal, and offshore engineering from Hohai University, Nanjing, China, in 2007 and 2010, respectively, where he is currently pursuing the Ph.D. degree in harbor, coastal, and offshore engineering. After his graduation, he worked at the Zhejiang Institute of Hydraulics & Estuary. His research interests include marine hydrodynamics, coastal sediment movement, and the interaction between waves and marine structures.

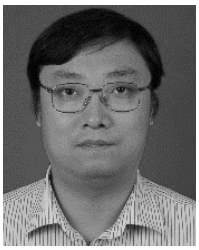

LIN MU received the B.S., M.S., and Ph.D. degrees in physical oceanography from the Ocean University of China, Qingdao, China, in 2000, 2002, and 2007, respectively. He is currently a Professor and Ph.D. Professor of physical oceanography with Shenzhen University, Guangdong, China. He has authored or coauthored over 20 scientific articles and four books. His research interests include physical oceanography: prevention and mitigation of marine disasters, maritime search and rescue, and emergency response management of offshore oil spills.